10.1071/CH10210_AC

Australian Journal of Chemistry 2010, 63(11), 1557–1564

SUPPORTING INFORMATION

Synthesis, structural, DFT and cytotoxicity studies of Cu(II) and Ni(II) complexes with 3-aminopyrazole derivatives*

Berta Holló,[A] Vukadin M. Leovac,[A] Petra Bombicz[B], Attila Kovács[C,D], Ljiljana S. Jovanović[A], Gordana Bogdanović,[E] Vesna Kojić,[E] Vladimir Divjaković[A], Milan D. Joksović[F], Katalin Mészáros Szécsényi[A,G]

[A]Faculty of Sciences, University of Novi Sad, Trg D.Obradovića 3, 21000 Novi Sad, Serbia

[B]Institute of Structural Chemistry, Chemical Research Center, Hungarian Academy of Sciences, P.O. Box 17, H-1525 Budapest, Hungary

[C]Research Group for Materials Structure and Modeling of the Hungarian Academy of Sciences, Budapest, University of Technology and Economics, H-1111 Budapest, Szt. Gellért tér 4, Hungary

[D]European Commission, Joint Research Centre, Institute for Transuranium Elements, P. O. Box 2340, 76125 Karlsruhe, Germany

[E]Institute of Oncology Sremska Kamenica, Institutski put 4, 21204 Sremska Kamenica, Serbia

[F] Faculty of Sciences, University of Kragujevac, R. Domanovića 12, 34000 Kragujevac, Serbia

[G]Corresponding author. Email: mszk@uns.ac.rs

Table of Contents

* Transition metal complexes with pyrazole-based ligands. Part 30.

Table 1. Intermolecular interactions in structures [Cu(*ampf*)Cl_2], 1, [Cu(*ampf*)MeOH$(NO_3)_2$]MeOH, 2 and [Ni(*ampf*)$(MeOH)_2NO_3$]NO_3, 3.

	D–H...A	Type	D–H [Å]	H...A [Å]	D...A [Å]	D–H...A [°]	Symmetry operation
1	N6–H6...O42	intra	0.88	2.20	2.828(5)	127	
	C7–H7...N10	intra	0.95	2.23	2.637(6)	105	
	N2–H2...Cl1	intra	0.88	2.55	3.036(4)	115	
	N11–H11...Cl2	dimer	0.88	2.26	3.131(4)	171	–*x*,–*y*,–*z*
	C121–H12A...Cl2	dimer	0.98	2.68	3.654(4)	173	*x*, –1/2–*y*, 1/2+z
	N2–H2…O42	chain *b*	0.88	2.45	2.973(4)	119	*x*, –1+y,z
	N6–H6…Cl2	chain *b*	0.88	2.57	3.218(4)	131	x,1+*y*, *z*
	C7–H7…Cl2	chain *b*	0.95	2.67	3.284(4)	123	*x*, 1+*y*, z
	C43–H43C...Cl1	intercolumn	0.98	2.71	3.505(5)	138	1–*x*,-*y*,–*z*
2	N6–H6...O42	intra	0.86	2.13	2.759(3)	129	
	C7–H7...N10	intra	0.93	2.27	2.667(4)	105	
	N6–H6...O501	dimer	0.86	2.22	2.900(3)	136	1–*x*, –*y*, 2–*z*
	N11–H11...O401	chain *b*	0.86	2.06	2.900(4)	164	1–*x*, 1–*y*, 2–*z*
	N11–H11...O403	chain *b*	0.86	2.51	3.225(4)	141	1–*x*, 1–*y*, 2–*z*
	O301–H301...O503	chain *c*	0.82	2.50	3.159(4)	138	
	O301–H301...O504	chain *c*	0.82	2.00	2.794(4)	164	
	N2–H2...O301	chain *c*	0.86	1.96	2.769(3)	156	1–*x*, –*y*,1–*z*
	C121–H12C...O403	intersheet	0.96	2.41	3.339(5)	163	1+*x*, *y*, *z*
3	N6–H6...O42	intra	0.88	2.11	2.755(2)	130	
	C7–H7...N10	intra	0.95	2.27	2.665(3)	104	
	N2–H2...O501	in asym unit	0.88	1.98	2.845(4)	167	
	O201–H201...O503	in asym unit	0.84	1.86	2.692(3)	168	
	O301–H301...O404	chain *a*	0.84	1.99	2.784(2)	157	–1+*x*, *y*, *z*
	N6–H6...O504	chain *b*	0.88	2.21	2.896(3)	135	*x*, 1+*y*, *z*
	C7–H7...O504	chain *b*	0.95	2.55	3.082(3)	115	*x*, 1+*y*, *z*
	N11–H11...O401	dimer	0.88	2.30	3.093(3)	151	2–*x*, 1–*y*, 1–*z*
	N11–H11...O403	dimer	0.88	2.30	3.074(3)	148	2–*x*, 1–*y*, 1–*z*

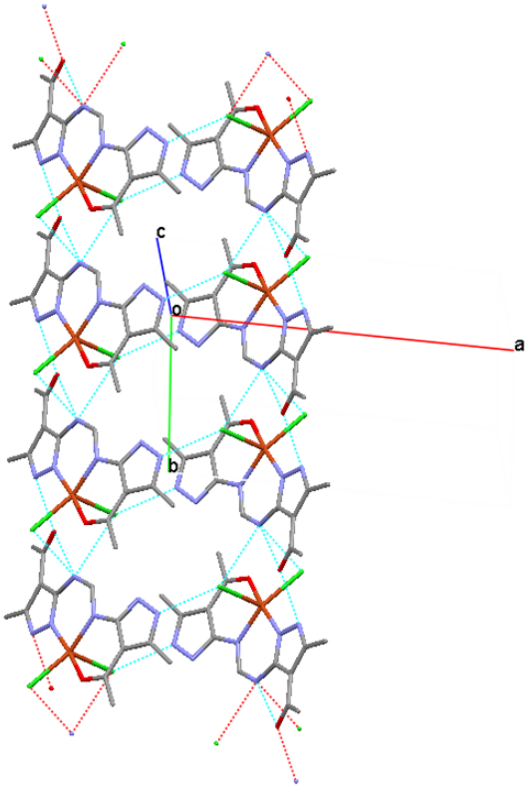

Fig. 1a. Packing arrangement in crystal **1** [1].

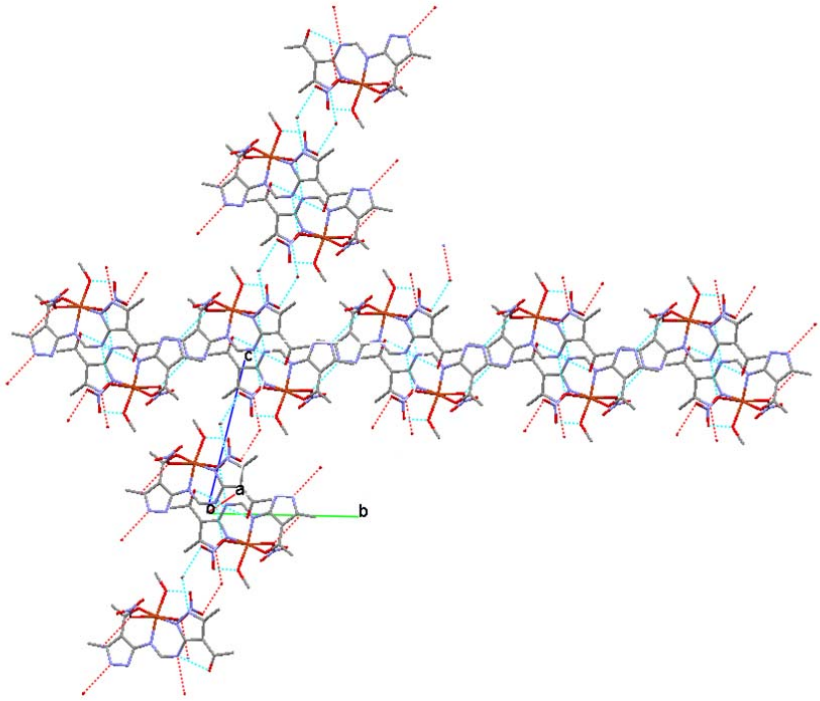

Fig. 1b. Packing arrangement in crystal **2** [1].

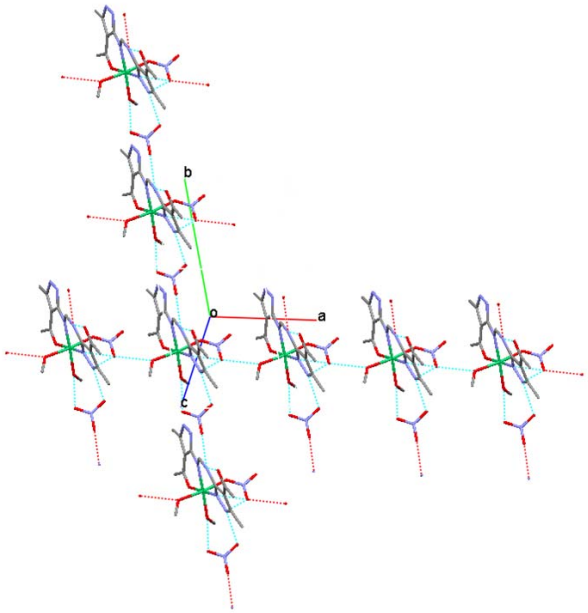

Fig. 1c. Packing arrangement in crystal **3** [1].

Computed geometry and vibrational frequencies

The computed metal-ligand distances are compiled in Table 2. The data reflect the main geometrical differences between the crystal structure obtained from the X-ray study and the isolated complex from the calculations. The agreement is farily good for the ligand bond lenghts. This implies the reliability of the computed IR data of *ampf*, corresponding to most of the bands in the IR spectrum. The agreement is worse for the metal-ligand distances. The M–N1 and M–O15 distances are still in fair agreement, but the M–N8 bonds and the bonds with the NO_3^- and MeOH ligands deviate up to 0.3 Å. The main reason of the deviations is that the computed geometrical data refer to the isolated complexes, therefore cannot take into account the crystal packing effects and hydrogen bonding interactions between neighboring complexes. The anions are involved in strong hydrogen bonding interactions with the neighboring complex molecules in the crystal. Therefore they occupy an intermediate position between two complexes. In the isolated molecule model of the computations, there is only one complex these ligands can coordinate to, so they can bind more strongly to the metal (by donor-acceptor interactions) and to the other ligands (by hydrogen bonding interactions) resulting in smaller distances.

Table 2. Comparison of selected experimental and computed bond distances (Å).

	1		**2**		**3**	
	Calculated	X-ray	Calculated	X-ray	Calculated	X-ray
N1=C5	1.318	1.322(5)	1.328	1.332(4)	1.325	1.317(3)
C5–N6	1.372	1.367(5)	1.383	1.372(4)	1.387	1.382(3)
N6–C7	1.345	1.341(5)	1.354	1.340(4)	1.346	1.338(3)
C7=N8	1.302	1.301(5)	1.295	1.302(4)	1.303	1.289(3)
N8–C9	1.413	1.414(4)	1.384	1.412(4)	1.398	1.411(3)
C14=O15	1.254	1.252(4)	1.250	1.247(4)	1.240	1.240(3)
M–N1	2.015	1.962(3)	2.000	1.962(3)	2.074	2.016(2)
M–N8	2.312	2.008(3)	2.252	1.978(3)	2.131	2.050(2)
M–O15	1.983	1.973(2)	1.972	1.955(2)	2.090	2.020(1)
Cu–Cleq	2.381	2.288(1)				
Cu–Clax	2.354	2.543(1)				
M–O401			2.092	2.381(3)	2.011	2.111(8)
$M–O301_{complex3}$					2.233	2.089(2)

M–O501 $_{complex2}$	2.058	2.539(3)		
M–O201	2.439	1.974(3)	2.084	2.065(2)

The full list of the IR absorption bands and their assignment are given in Table 3 while the spectra are shown in Figure 2. The assignment of the absorption bands was aided by the computed vibrational frequencies and IR intensities, while the computed normal modes were visualized by the GaussView 4.1 program [2].
The most notable feature is the high frequency of the stretchings of the formally CN and NN single bonds which can be attributed to the partial double-bond character of these bonds due to conjugation of the neighboring π bonds and the lone pairs of nitrogens. These bands appear at very close wavenumber values in the spectra of the three complexes, in agreement with the identical donor-acceptor interaction of the *ampf* ligand with the metals. The most important information gained from the far-IR range are the metal-ligand vibrations, which correlate well with values published for related complexes in Ref. [8].

Table 3. Characteristic bands[A] of the FT-IR spectra of 1, 2 and 3 and their assignments on the basis of the DFT calculations

Experimental	Calculated	Intensity	Assignment[B]
[Cu(ampf)Cl_2] (**1**)			
3241s	3657	112	νNH
3151m	3477	383	νNH
3126m	3411	366	νNH
3074m	3171	7	$\nu_{as}CH_3$
3040m	3152	8	νCH
3020m	3145	7	$\nu_{as}CH_3$
3000m	3132	12	$\nu_{as}CH_3$
2967m	3118	5	$\nu_{as}CH_3$
2919m	3061	21	$\nu_{s}CH_3$
2860m	3058	2	$\nu_{s}CH_3$
1641s	1700	753	νC=O
1605s	1681	184	νC=N
1578s	1633	362	νring, βN6H, νC=O
1548s	1606	483	νC7−N6
1529m	1587	45	νring
1504s	1571	119	νring, βNH_{ring}
1466s	1496	464	νring, $\delta_{as}CH_3$
1440m	1497	30	$\delta_{as}CH_3$
1412s	1468	149	$\delta_{as}CH_3$,
1355s	1397	18	$\delta_{as}CH_3$, βCH, βNH
1312m	1339	88	νring
1212m	1260	50	νN−N
1159m	1218	41	νN−N, νC7−N6
1096s	1118	58	νring, $\nu C-CH_3$
1036w	1061	5	$\delta_{r}CH_3$
1005w	1044	2	$\delta_{r}CH_3$
973m	981	46	$\nu C-CH_3$
964m	969	48	$\nu C-CH_3$
913m	924	16	δring, βN−CH−NH
799s	786	26	γN6H
773m	770	32	τring, γN6H
743m	768	26	γN6H, τring
732m	748	40	γNH_{ring}
712s	727	32	γNH_{ring}
666m	668	35	γNH_{ring}
587w	583	15	δring

575w	562	40	γNH_{ring}, τring
449w	452	5	τring, γC_{ring}−N
343w	368	13	νCu−N8, νCu−O15, βC−C−CH_3
302sh	314	13	γC−N8
273m	283	51	νCu−Cl
233w	222	15	νCu−Cl
172m	178	2	βN8−Cu−O15
140m	146	9	βN1−Cu−N8
106w	121	17	$\gamma CuCl_2$
95sh	100	9	τCH_3
70sh	62	11	βCl−Cu−Cl

[Cu(ampf)(MeOH)$(NO_3)_2$]MeOH (**2**)

3485s	3582	714	νNH, νOH
3229s	3417	542	νNH, νOH
3089sh	3107	56	$\nu_{as}CH_3$
3042sh	3152	8	νCH
2973sh	2995	107	ν_sCH_3
1643s	1721	200	νC=O42
1610s	1688	902	νC=N8
1601s	1663	296	νC=O15
1580sh	1636	445	νring, βN6H, νC=O
1552s	1598	428	νC7−N6
1529w	1584	124	νring
1504s	1576	352	$\nu_{as}NO_3$, βOH
1467s	1543	75	νring
1453m	1506	212	νC5−N6, $\delta_{as}CH_3$
1413m	1492	238	νC4−C41, $\delta_{as}CH_3$
1384vs	1339	541	$\nu_{as}NO_3$
1354sh	1406	17	νring
1330sh	1388	22	βC7H
1207m	1255	48	νN−N, νC9−N8
1159w	1220	16	νN−N, νC9−N8
1100m	1124	47	νring, νC−CH_3
1063w	1076	99	ν_sNO_3, δ_rCH_3
1042w	1065	91	νC−O, ν_sNO_3, δ_rCH_3
1007w	1054	59	νC−O, ν_sNO_3, δ_rCH_3
975m	989	57	νC−CH_3
914m	926	15	βNH−CH−N, δring, νC−CH_3
850-650vbr	949	207	τOH
839w	821	71	δNO_3, γNH
794m	792	18	γNH_{ring}, δring, νC9−N8
773w	778	17	βC5−N6−C7
703w	746	17	τOH, δNO_3, δring
671m	676	31	βC−C=O
589m	597	26	δring
581m	572	28	γNH_{ring}
451m	455	5	τring, γC5−N6
340w	374	16	νCu−O, νCu−N8
303w	328	11	νCu−N8, γC7H
279w	308	42	$\nu Cu-O_{NO3}$
253	258	10	$\nu Cu-O_{NO3}$
202m	224	15	βO−Cu−O, $tw NO_3$
188	188	9	βN8−Cu−O, τCH_3
128m	131	6	γCuO−CH_3

97w	98	12	βO−Cu−O, τCH_3
56w	52	3	twNO_3

$[Ni(ampf)(MeOH)_2(NO_3)]NO_3$ (**3**)

3355s,br	3385	509	νNH
3254s,br	3010	1901	νNH, νOH
3086sh	3172	3	νCH
3043sh	3122	29	$\nu_{as}CH_3$
3007sh	3057	186	$\nu_{s}CH_3$
1650sh	1714	285	νC=O42
1637sh	1707	496	νC=O15
1617s	1677	639	νC=N8
1594sh	1645	127	νring, βN6H, νC=O
1553s	1616	509	νC7−N6
1502m	1556	81	βOH, νN−O
1461s	1497	489	νC4−C41, $\delta_{as}CH_3$
1416m	1469	81	$\delta_{as}CH_3$
1384s	1365	474	$\nu_{as}NO_3$
1359sh	1398	51	βC7H, $\delta_{s}CH_3$
1280w	1311	72	νC5−N6, νring, βN6H
1204m	1254	65	νC9−N8, νN−N
1164w	1214	55	νN−N, νC9−N8
1098m	1119	62	νring, νC−CH_3
1045w	1074	69	$\nu_{s}NO_3$
1031w	1061	86	$\nu C-O_{MeOH}$
1023w	1055	63	$\nu_{s}NO_3$, $\nu C-O_{MeOH}$
1010w	1036	113	$\nu C-O_{MeOH}$
973w	982	121	νC−CH_3, δCH_3, γNH_{ring}, βNH−CH−N
962w	976	127	γNH_{ring}
913w	924	45	βN−C−N, δring
870-550vbr	1021	20	τOH
839w	843	66	γN6H
825w	824	33	γNO_3
795w	794	21	γN6H, δring, νC5−N6
768w	777	15	βN−C−N
663m	663	36	βC−C=O
582sh	611	217	τOH_{axMeOH}
574w	590	17	δring
529w	567	36	γNH_{ring}, γC−C=O
444w	455	11	τring, γC5−N6
381w	399	24	$\nu Ni-O_{eqMeOH}$
333m	327	19	$\nu Ni-O_{axMeOH}$, $\nu Ni-O_{NO3}$, νNi−N8
286w	309	27	$\nu Ni-O_{axMeOH}$, $\nu Ni-O_{NO3}$
274w	287	37	$\nu Ni-O_{axMeOH}$, $\nu Ni-O_{NO3}$
244w	255	27	νNi−N8
210m	218	18	νNi−N8
184w	189	11	$\beta N8-Ni-O_{eqMeOH}$, τCH_3
129m	129	2	τCH_3, γ$NiO-CH_{3(axMeOH)}$
97m	93	4	γ$C_{ring}-CH_3$, $\beta N-Ni-O_{eqMeOH}$
70m	64	2	twNO_3

[A] In cm^{-1}. The abbreviations vs, s, sh, m, w, br mean very strong, strong, shoulder, medium, weak and broad, respectively.

[B] Major contributions deduced from visual observation of the computed vibrations. The abbreviations M, as, ν, δ, β, tw, γ, τ mean metal (Cu or Ni), asymmetric, stretch, deformation, bend, twist, wag and torsion, respectively.

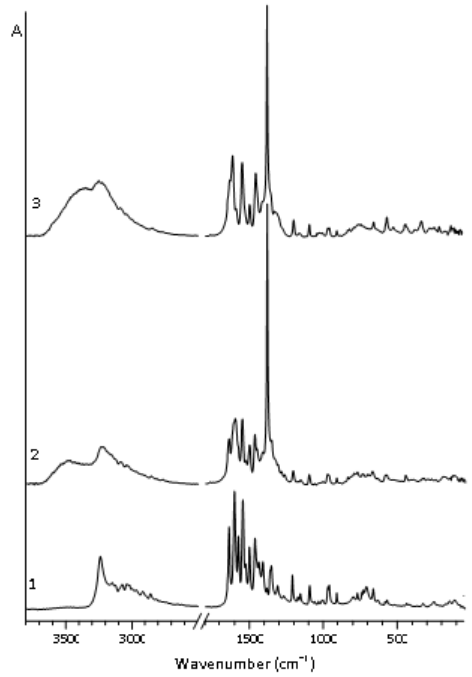

Fig. 2. FT-IR spectra of **1**, **2** and **3**.

The mid-IR range consists of the ligand vibrations, from which the asymmetric stretching of the NO_3^- group (in **2** and **3**) gives rise to the highest-intense band at around 1380 cm^{-1}. The *ampf* ligand provides several strong bands in this region due to CO, CN, NN, NO stretching, and OH and NH bending vibrations, in agreement with the identical donor-acceptor interaction of the *ampf* ligand with the metals.

Table 4. Additional natural atomic charges[A] and second-order perturbation energies[B]

		Atomic charges		
Fragment	**Atom**	**1**	**2**	**3**
Cl^-	Cleq	–0.588		
	Clax	–0.573		
NO_3^-	O501		–0.517	
	O401		–0.544	–0.573
MeOH	O201		–0.810	–0.806
	O301			–0.749
		Charge transfers to the metals		
Cl^- → M				
$E^{(2)}$ LP(Cleq) → M		302.3		
$E^{(2)}$ LP(Clax) → M		360.4		
Σ $E^{(2)}$ LP(Cl) → M		662.7		
NO_3^- → M				
$E^{(2)}$ LP(O401) → M			210.7	222.4
$E^{(2)}$ LP(O501) → M			214.2	

$\Sigma E^{(2)}$ LP(O) → M	424.8	222.4
MeOH → M		
$E^{(2)}$ LP(O201) → M	70.1	153.4
$E^{(2)}$ LP(O301) → M		107.1
$\Sigma E^{(2)}$ LP(O) → M	70.1	260.5

[A] The atomic charges are given in electrons.

[B] M means the metal (Cu or Ni) in the complexes. Second-order perturbation energies ($E^{(2)}$ donor → acceptor, kJ/mol). The abbreviation LP means the lone pairs of the atoms. Items starting with Σ represent the summarized quantities for the species. For the numbering of atoms see Figures 1a – c in the main part of the paper.

Electronic spectra

Spectra of the complexes were recorded in MeOH in the spectral range 220 – 1400 nm. The complexes **2** and **3** are readily soluble at 1 mmol/dm^3 concentration level, but not **1**. In order to improve that, the complex **1** was mildly heated (to about 40 ^{o}C) for app. 15 minutes. The color of solutions of Cu(II) complexes was green and that of the Ni(II) compound was very light blue.

The spectra of Cu(II) complexes are, generally, similar. In the λ range of 220-400 nm three well resolved absorption bands appear. The bands at ~233 nm and ~266 nm, which are present also in the spectrum of the starting ligand *aamp,* belong to π→π* transitions (pyrazolyl-based). A slight blue shift of the bands in the spectra of **1** and **2** was observed. This was not the case with [Co(*ampf*)$(MeOH)_2NO_3]NO_3$ complex [3] where the bands in the ligand absorption range are considerably red-shifted and molar absorptivities several times less intense than those of *aamp***.** These facts reflect a greater influence of the Co(II) on the coordinated ligand in the complex.

The third band, appearing at about 320 nm for both Cu(II) complexes, can be ascribed to LMCT. Since this band is rather broad and intense, it seems reasonable to assume that it is composed of two close absorptions, probably of $\pi_1, \pi_2 \rightarrow$ Cu(II). Such close transitions are not rare at pyrazole-type Cu(II) complexes [4]. Furthermore, for the complex **1** in this spectral range (λ~330 nm) also Cl → Cu(II) band can be expected [5]. Finally, the low-energy bands (λ >600 nm) in the spectra of both complexes can be attributed to *d-d* transitions. Having in mind the observed similarities in the colour and spectral characteristics of the complexes **1** and **2**, and also of conductivity data for **2** which point to a partial dissociation of the NO_3 ligands, it can be supposed that both complexes have a rather distorted, probably square-pyramidal Cu(II) environment.

The spectrum of Ni complex (**3**) in its high energy region is quite similar to that of the Cu(II) complexes and so are the corresponding assignments of the bands. Three other, rather weak absorptions in the range λ>590 nm (*d-d* transitions) and a very light blue colour of their solution may be an evidence of a preserved distorted octahedral Ni(II) environment in methanolic solution.

Thermal analysis

There are few data connecting the structure of the compounds with their thermal behavior in spite of the strong relationship between the decomposition pattern and the structure of the compounds. This is not surprising, because beside the structure of the compound, its macroscopic properties as well as the experimental conditions affect the thermal decomposition.

The thermal stability of the complexes is found to be the same in both gas carriers. The decomposition mechanism in air and nitrogen above 400 ^{o}C for **1** and for the nitrate complexes **2** and **3** above 200 ^{o}C, takes a different course, being more intensive in air.

Compound **1** is thermally stable up to 255 ^{o}C. Its endothermic decomposition begins with a DTG maximum at 266 ^{o}C and a DTA minimum at 270 ^{o}C and proceeds further by exothermic processes in nitrogen, too. The decomposition of **1** is continuous in the whole temperature range. Even with the SWI technique no intermediates could be isolated. The mass loss up to the first minimum of the DTG curve could fit the loss of HCl or it would correspond to the fragmentation of the side chains of the organic ligand. To decide which process is more likely we performed a qualitative reaction, the gases evolved during the decomposition bubbling through an acidic $AgNO_3$ solution. As no precipitation was observed, the HCl evolution could be excluded. Hence the decomposition begins with the departing of organic fragments.

In the lack of coupled measurements, only the mechanism of solvent evaporation can be discussed. Usually the decomposition of isostructural compounds is very similar [6,7]. On the other hand, similar decomposition curves do not necessarily belong to isostructural compounds. Sometimes even very small structural differences

may be detected by means of TA. The thermal curves of the MeOH evaporation of **2** and **3** are presented in Fig. 3. As is evident, the mechanism of the solvent loss is almost identical, in spite of the fact that in **3** both methanol molecules belong to the inner coordination sphere while in **2** only one MeOH is coordinated to the metal centre. The evaporation of MeOH begins at 65 ^{o}C (**2**) and at 67 ^{o}C (**3**) despite of their different crystallographic position. The solvent evaporation is a complex process and takes place in two well separated steps. It is completed at 112 and 128 ^{o}C for **2** and **3**, respectively. The mass loss of solvent evaporation to the corresponding DTG minimum, within experimental errors, agrees with the theoretical one (calcd.): **2,** 13.0% (11.24%); **3,** 11.0% (11.97%). The complexes without solvent are not stable and the decomposition proceeds exothermically at a slow, steady rate in both atmospheres. In spite of the similarities in MeOH evaporation, the rate of the process is significantly higher and begins at somewhat lower temperature in **2**. This complex contains MeOH as crystal solvent referring probably to its lower bonding energy, including its stabilization by H-bonds and/or an easier diffusion through the lattice.

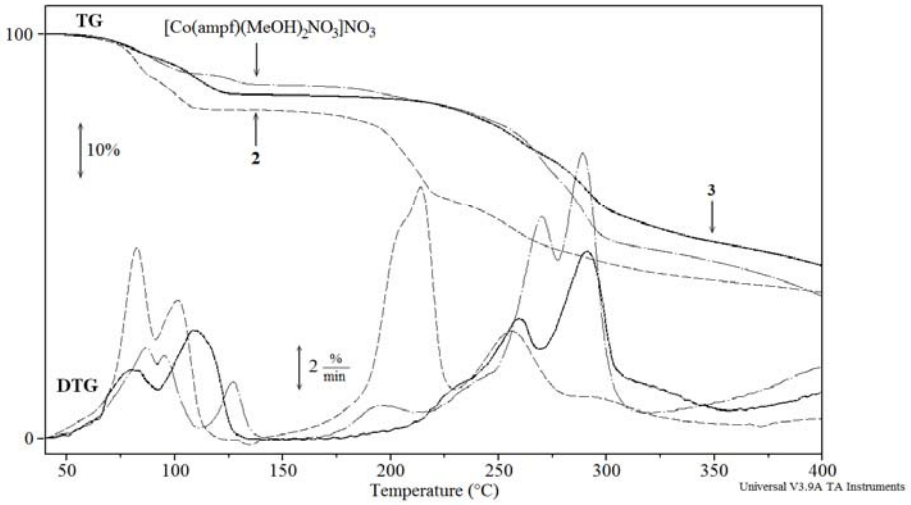

Fig. 3. TG-DTG curves of **2**, **3** and [Co(*ampf*)$(MeOH)_2NO_3]NO_3$ [3].

Supporting the complexity of the task to correlate the structural data with the thermal decomposition mechanism, a good example is the unexpected similarity between the mechanisms of the solvent evaporation of **2** and **3**, compounds with similar composition, but different crystal structure. It cannot be explained on the basis of the structural data only. In addition, they do not explain the significant differences in thermal decomposition of isostructural [Co(*ampf*)$(MeOH)_2NO_3]NO_3$ [3] and **3** complexes. TA data for the cobalt(II) complex were repeated using the equipment and experimental conditions described in this paper. Its decomposition pattern did not change. The slight differences in are due to the better resolution of the instrument and to lower sample mass. The lower solvent content is the consequence of the storage conditions. As the interactions in Co(II) and Ni(II) crystals are similar, the different thermal behavior may be also a consequence of the different redox properties of Co(II) and Ni(II).

In vitro biological activity

The synthesized compounds and the ligand precursor (*aamp*) were tested for their biological activity against human myelogenous leukaemia K562, colon adenocarcinoma HT29, cervix carcinoma HeLa and normal foetal lung fibroblasts, MRC-5. In vitro cytotoxicity was evaluated by sulforhodamine B (SRB) assay after 48h-treatment of cells. Table 3 shows the cytotoxicity of *aamp* and the complexes against four cell lines for the target compounds including Doxorubicin (Dox) as a reference drug.

Table 3. *In vitro* cytotoxycity of *aamp*, 1, 2 and 3

Compounds	IC_{50}, μM[A]			
	K562	**HeLa**	**HT29**	**MRC-5**
aamp	47.3	>100	0.6	>100
1	>100	20.2	89.0	>100
2	50.7	88.3	14.3	>100
3	>100	>100	10.13	>100
Dox	0.4	1.2	0.5	0.3

[A] IC_{50} is the concentration of compound required to inhibit the cell growth by 50% compared to an untreated control

The cytotoxic activity of the *aamp* ligand and *ampf* complexes **1**, **2**, **3** against the selected test lines is very different (see data in Table 3). The common feature of all compounds is that their cytotoxicity against human non-tumor MRC-5 cell line is negligible. The cytotoxicity of *aamp* for HT29 is comparable to that of the Doxorubicin, but without cytotoxic effect against MRC-5 cell line. *Aamp* shows low or no activity against K562 and HeLa cell line, respectively. The activity of **1** is moderate against HeLa cell line but negligible against the two other tumor cell lines. This feature of **1** might be a consequence of the absence of the nitrato group. According to literature data [9] in some cell lines copper(II) is reduced to copper(I) that induces production of reactive oxygen species (ROS) with significant cytotoxic effect against human tumor cells. This reduction could be prevented by the presence of nitrato group in **2**. However, the reason for the different cytotoxicity of the compounds against HeLa has not yet been determined. For HT29 line the complexes show moderate cytotoxicity, in the increasing order of **1** < **2** < **3**. The activity of the complexes is very low or negligible against K563 tumor cells.

Experimental for cytotoxicity in vitro

Three human tumor cell lines and one human non-tumor cell line were used in the study: K562 (Chronic myelogenous leukemia), HeLa (Epitheloid carcinoma of cervix), HT29 (Colon adenocarcinoma), and MRC-5 (Lung foetal fibroblasts). The cells were grown in RPMI 1640 (K562 cells) or Dulbecco's modified Eagle's medium (DMEM) with 4.5% of glucose (HeLa, HT29, and MRC-5 cells). Media were supplemented with 10% of fetal calf serum (FCS, NIVNS) and antibiotics: 100 IU/cm^3 of penicillin and 100 μg/cm^3 of streptomycin (ICN Galenika). All cell lines were cultured in flasks (Costar, 25 cm^2) at 37 ^oC in the 100% humidity atmosphere and 5% of CO_2. Only viable cells were used in the assay. Viability was determined by dye exclusion assay with Trypan blue. Cytotoxicity was evaluated by colorimetric SRB assay after Skehan *et al.* [10]. Briefly, single cell suspension was plated into 96-well microtitar plates (Costar, flat bottom): $1 \cdot 10^4$ of K562 and $5 \cdot 10^3$ of HeLa, HT29, and MRC5 cells, per 180 cm^3 of medium. Plates were preincubated 24 h at 37 ^oC, 5% CO_2. Tested substances at concentration ranging from 10^{-8} mol dm^{-3} to 10^{-4} mol dm^{-3} were added to all wells except to the control ones. After the incubation period (48 h /37 ^oC /5% CO_2) SRB assay was carried out as follows: 50 μl of 80% trichloroacetic acid (TCA), was added to all wells; an hour later plates were washed with distilled water, and 75 μl of 0.4% SRB was added to all wells; half an hour later plates were washed with citric acid (1%) and dried at room temperature. Finally, 200 μl of 10 mmol TRIS (pH=10.5) basis was added to all wells. Absorbance was measured on the microplate reader (Multiscan MCC340, Labsystems) at 540/690 nm. The wells without cells, containing compete medium only, were taken as blank. Cytotoxicity was calculated according to the formula $(1 - A_{test}/A_{control}) \times 100$ and expressed as a percent of cytotoxicity (CI%).

References

[1] C. F. Macrae, I. J. Bruno, J. A. Chisholm, P. R. Edgington, P. McCabe, E. Pidcock, L. Rodriguez-Monge, R. Taylor, J. van de Streek and P. A. Wood, *J. Appl. Cryst.* **2008,** *41*, 466.

[2] GaussView, Version 4.1, R. Dennington II, T. Keith, J. Millam, Semichem, Inc., *Shawnee Mission*, KS, 2007.

[3] V. M. Leovac, Z. D. Tomić, A. Kovács, M. D. Joksović, Lj. S. Jovanović, K. Mészáros Szécsényi, *J. Organomet. Chem*. **2008**, *693*, 77.

[4] B. P. Lever, Inorganic Electronic Spectroscopy, Part 1, 1967, pp. 353–362 (Sec. Edition, Elsevier, Russian translation).

[5] E. I. Solomon, K. W. Penfield, D. E. Wilcox, *Struct.& Bonding* **1983**, *53*, 1.

[6] Z. Z. Rzączyńska, M. Woźniak, W. Wołodkiewicz, A. Ostasz, S. Pikus, *J. Therm. Anal. Cal*. **2008**, *91*, 951.

[7] S. A. AbouEl-Enein, *J. Therm. Anal. Cal*. **2008**, *91*, 929.

[8] K. Nakamoto, *Infrared and Raman Spectra of Inorganic and Coordination Compounds. Part B: Applications in Coordination, Organometallic and Bioinorganic Chemistry*, **1997**, pp. 24–26, 58–59, 87, 184 (Wiley & Sons, New York).

[9] R. Alemón-Medina, M. Brena-Valle, J. L. Munoz-Sanchez, M. I. Gracia-Mora, L. Ruiz-Azuara, *Cancer Chemother. Pharmacol.* **2007**, *60*, 219.

[10] P. Skehan, R. Storeng, D. Scudiero, A. Monks, J. McMahon, D. Vistica, J. T. Warren, H. Bokesch, S. Kenney, M. R. Boyd, *J. Natl. Cancer Inst.* **1990**, *82*, 1107.